Material adhesion and stresses on friction stir welding tool pins

M. Mehta[1], A. De*[1] and T. DebRoy[2]

During friction stir welding, polygonal tool pins experience severe stresses and, under certain conditions, loss of functionality due to adhesion of plasticised material on their surfaces. The extent of adhesion is analysed for various pin geometry and welding conditions based on the theory of machining. The effective stresses on the polygonal pins are evaluated following the principles of mechanics. The results show that the polygonal pins with fewer sides can avoid permanent adhesion of plasticised material at higher weld pitch, which is defined as a ratio of welding speed and tool rotational speed. The computed pin geometries for minimum adhesion are compared with the pin profiles recommended by various investigators based on independent experiments. The computed stresses show that pins with larger number of sides will experience lower stresses for any given set of welding variables.

Keywords: Friction stir welding, Tool pin geometry, Polygonal pin, Tool durability

Introduction

During friction stir welding (FSW), the shoulder diameter and pin geometry affect the welding process, and the microstructure and the properties of the joint.[1,2] The role of tool shoulder has been extensively discussed in a recent review of FSW tools.[3] In the previous studies of pin geometry,[4–23] emphasis has been placed on the testing and characterisation of welds. Apart from the pins of circular cross-section,[8,17–20] various polygonal cross-sections such as triangle,[4–8] square,[9–16] and hexagon[21] shapes have been recommended in different studies for various welding conditions.

Several investigations[4–8] indicated that a pin with a triangular cross-section increased the flow of plasticised material compared to a cylindrical pin. Defect-free welds were also obtained with pins of square cross sections.[9–16] For the FSW of AA2014, superior tensile property of the joint was achieved with a hexagonal pin,[21] although the joint properties did not show significant differences for square, pentagon and hexagon cross-sections. In addition, sound welds were also achieved with pins of circular cross-section.[8,17–20] Because of the conflicting previous recommendations, no unified methodology or model now exists to select an appropriate pin cross-section.

The tool pin facilitates movement of plasticised material during FSW.[4–23] Under certain conditions, plasticised materials may adhere to the tool pins locally.[24–29] Such adhesion impairs the pin's ability to facilitate transport of the plasticised materials. The flow of plasticised material on the pin faces is similar to the flow of chips in machining.[24] Sticking of chips on the cutting tool is particularly pronounced for softer materials at low speeds.[25–29] Inappropriate selection of welding speed and tool rotational speed may also lead to permanent adhesion of plasticised material on the flat faces of the polygonal pins and distorts flow of plasticised materials around the pin.[9]

The tool pins have a much lower stiffness compared to the shoulder and need to endure severe stresses[30–32] during FSW which affect its durability.[31] The cross-sections of the tool pin affect the stresses experienced by the pin. Although stresses on the circular cross sections were examined in previous studies,[30–32] the stresses on various polygonal pins were not evaluated. There is a need to study how the various cross-sections of the tool pin and the welding conditions affect the adhesion of plasticised materials and stresses on the tool pin.

This is the first paper to investigate the conditions necessary to avoid undesirable adhesion of material on the tool pin by appropriate selection of both the pin geometry and the welding variables following principles of machining. The effectiveness of the approach is examined by comparing the computed results with those experimentally determined in multiple independent investigations. Furthermore, the effective stresses on pins of various polygonal shapes which affect its durability are evaluated based on the principles of mechanics.

Theoretical formulation

The flow of plasticised material over the polygonal pin faces during a steady-state FSW operation can be considered analogous to the chip flow over tool rake face in typical machining of metallic materials (Fig. 1). In contrast to free flow of chips in machining, the plasticised material in FSW undergoes a restricted flow and is consolidated to form the joint. The flow of deformed chips in machining results an extent of sticking (S) and sliding (L) along the

[1]Department of Mechanical Engineering, Indian Institute of Technology Bombay, Mumbai 400076, India
[2]Department of Materials Science and Engineering, The Pennsylvania State University, University Park, PA 16802, USA

*Corresponding author, email amit@iitb.ac.in

Published by Maney on behalf of the Institute
Received 7 March 2014; accepted 10 May 2014
DOI 10.1179/1362171814Y.0000000221

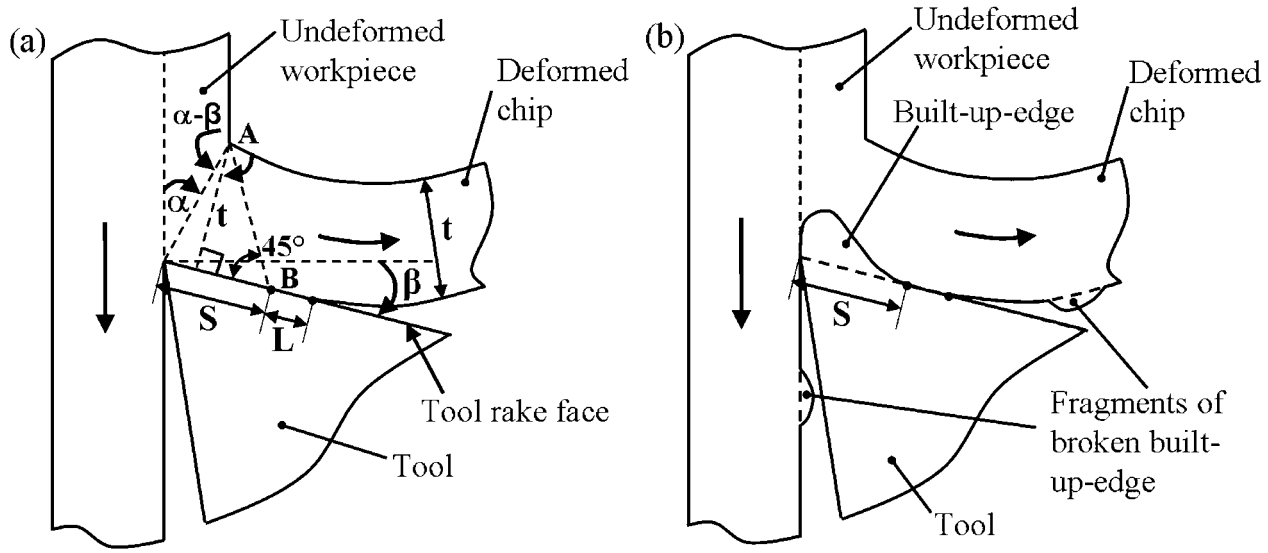

1 Schematic *a* geometry of deformed chip and *b* built-up edge on tool rake face in typical orthogonal machining with α=shear angle, β=rake angle, *t*=deformed chip thickness, *S*=sticking and *L*=sliding lengths[25]

tool-chip interface[25] with the former leading to a stagnant region and built-up edge (Fig. 1*b*) due to adhesion at high pressure and temperature. The built-up edge modifies the tool pin profile, results in a localised hot spot and promotes interfacial cracks and pitting due to differential thermal contractions between sticking chip and tool during cooling.[26,27] An appropriate choice of the tool geometry and machining conditions can improve chip flow, reduce the sticking of chips on the cutting tool and enhance tool life.[26–28]

In FSW, each edge and face of a polygonal pin is similar to the tool cutting edge and its rake face in conventional machining. The chips in machining are considered to undergo plastic deformation followed by shear fracture along a plane whose orientation angle (α) (Fig. 1*a*) is commonly estimated using the Lee and Shaffer relation as[25]

$$\alpha = (\pi/4) + \beta - \gamma \tag{1}$$

where γ is the mean friction angle along the tool-chip interface with $\tan\gamma \approx 0{\cdot}5$. The term β is the rake angle that depicts the orientation of the normal to the cutting velocity vector at the cutting edge with the tool rake face. The sticking length (*S*) along the tool-chip interface is estimated commonly using Abuladze's relation with the assumption that the boundary of the plasticised chip region (AB) meets the rake face at 45°(Fig. 1*a*) as[25]

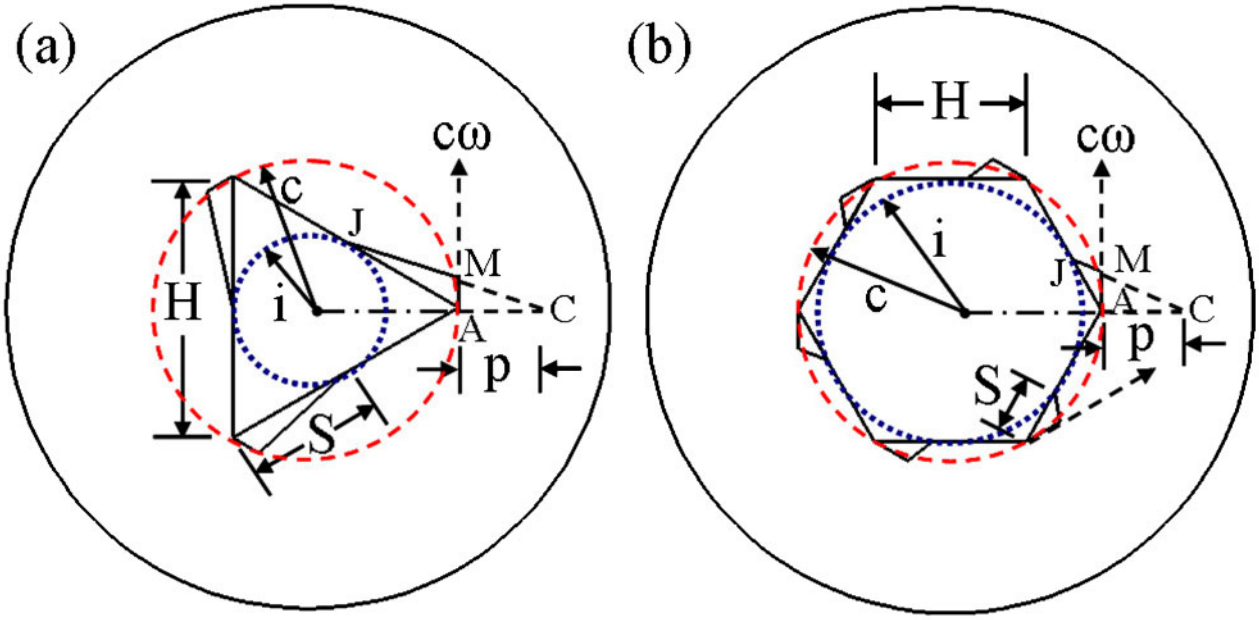

2 Schematic diagram showing shoulder (outer radius) and adhesion of plasticised material on pin sides for *a* triangular and *b* hexagon pin profiles where *H*=pin side length, *cω*=tangential velocity vector, and *S*=sticking length on pin side. Blue dotted and red dashed lines depict incircle and circumcircle, respectively

$$S = t \times [1 + \tan(\alpha - \beta)] = t \times [1 + \tan(\pi/4 - \gamma)] = 4t/3 \quad (2)$$

where t refers to the deformed chip thickness.

Figures 2*a* and *b* depict schematically the rake angle, β, on triangular and hexagonal pin cross-sections, respectively. Unlike in conventional machining, the flow of plasticised material along the polygonal pin faces will be affected by the combined rotational and linear motions of the FSW tool. The sheared plasticised material adjacent to the tool pin corresponds to the deformed chip and its thickness t can be estimated as

$$t = c - i + p \quad (3)$$

where c and i are respectively the circumradius and inradius for the polygonal pin profile, respectively, and p is the weld pitch, i.e. the linear distance travelled by the tool pin in each revolution. For a stationary pin with flat face, a maximum clearance of $c-i$ is available on each pin face for the passage of the plasticised material. The linear motion of the tool will further lead to an advancement of the pin by a distance p per unit revolution of the tool. The maximum clearance for the passage of plasticised material over each pin face will therefore be $c-i+p$.

The adhesion of the plasticised material on pin surfaces is explained in Fig. 2 for triangular and hexagonal pins. The sticking length[29] on the flat surface is AJ. The cross-section of the sticking region is taken as the triangle AJM for simplicity. One of its sides, AM, is along the direction of tangential velocity at A. The location of the point J depends on the weld pitch, p. The point C is at a distance p from the circumradius of the pin. The point M is located by the intersection of line CJ with the direction of tangential velocity. The total sticking length along the entire pin periphery of a polygonal pin of N sides can therefore be estimated using equations (2) and (3) as

$$S \times N = \frac{4}{3}(c - i + p) \times N \quad (4)$$

To avoid excessive sticking along the pin periphery and retain the original pin profile for continuous welding of longer weld seams, the total sticking length, S × N, along the pin periphery needs to be minimised as

$$\frac{\mathrm{d}(S \times N)}{\mathrm{d}N} = 0, \text{ i.e. } N_P = \frac{\pi}{2p^{1/2}} \times \left[c + \left(c^2 - 2pc\right)^{1/2}\right]^{1/2} \quad (5)$$

where N_P is the optimum number of polygonal pin sides for a given c and p. A derivation of equation (5) is presented in the Appendix.

Apart from the adhesion of the plasticised material, the performance of the tool pin is also affected by the stresses it endures. The tool pin experiences combined bending and torsion due to the simultaneous translational and rotational motions through the plasticised workpiece material. As a result, the pin will experience normal, σ_B, and shear, τ_B, stresses due to bending and a shear, τ_T, stress due to torsion. The resultant maximum shear stress, τ_{max}, at any point on a polygonal pin profile can be estimated following the Tresca's yield criteria as[30–33]

$$\tau_{max} = \left[\left(\frac{\sigma_B}{2}\right)^2 + (\tau_B + \tau_T \cos\lambda)^2 + (\tau_T \sin\lambda)^2\right]^{1/2} \quad (6)$$

where λ is the angle between τ_T and τ_B, measured in a counter-clockwise direction from τ_B to τ_T. A detailed methodology to estimate the component of stresses (σ_B, τ_B and τ_T) and τ_{max} for circular and polygonal pin profiles are already reported elsewhere[30–32] and are not repeated here. Subsequently, a *durability index* of a tool can be estimated as the ratio of the shear strength of the tool material and the corresponding τ_{max}.[30–32]

Results and discussion

Volume of plasticised material stirred by pin

An important function of the tool pin is the stirring of the plasticised material as the tool moves forward. An approximate assessment of the volume of plasticised material may be made by considering the inradius, i, and circumradius, c, of the pin and the distance it moves per unit revolution, p. The shear volume for a stationary rotating pin can be estimated as the volume of the truncated cone, $\pi\, l_P(r_S - c)^2/2$, formed by joining the shoulder and the pin peripheries and shown schematically in Fig. 3*a*, and the cylindrical volume of the sweep, $\pi\, l_P(c - i + p)^2$, because the inradius is smaller than the circumradius of polygonal pins and the pin is moving. As a result, the total shear volume can be approximated as

$$V_S = \pi l_P (r_S - c)^2/2 + \pi\, l_P (c - i + p)^2 \quad (7)$$

The inradius and the circumradius are the same for a circular pin while $c-i$ will be non-zero and decrease with the increasing the number of sides for a regular polygonal pin. Therefore, the average volume of the plasticised material around a polygonal pin is larger than a circular pin and would decrease with increasing the number of pin sides for a given c and p. Figure 3*b* shows an estimate of the average volume of the plasticised material around FSW tools with a circular and polygonal pins of N=3 to 6 for a given set of FSW conditions.[21] Figure 3*b* indicates that a triangular pin can stir a greater material volume compared to a circular as well as polygonal pins of higher number of sides, which has been also confirmed by independent experiments.[21]

Computed optimum polygonal pin cross-sections

For a given set of FSW conditions, the optimum polygonal pin profile will result in minimum adhesion of plasticised material around the entire pin periphery. Figure 4 shows that the sticking length, S, decreases with increasing number of pin sides, N. However, the total sticking length, $S \times N$, first decreases, reaches a minima and increases thereafter with increasing N. The decrease in S with increasing N is attributed to the corresponding decrease in $c-i$. Figure 4*a and b* shows the effects of weld pitch. For a pitch of 0·2 mm rev^{-1}, the optimum pin cross-section is found to be a regular octagon. When the weld pitch is increased to 0·6 mm rev^{-1}, the optimum cross-section changes to a regular pentagon. Thus, a polygonal pin of fewer sides becomes optimum as the weld pitch, p, increases. Equation (5) also gives the same answers from an analytical expression as expected.

Table 1 lists a large selection of the available data on the effects of various circular and polygonal pin cross-sections on the weld properties and the suggested optimum pin profile in each case. The values of the optimum number of pin sides computed from equation (5) are also shown in Table 1 for each case. The suggested pin profiles from the

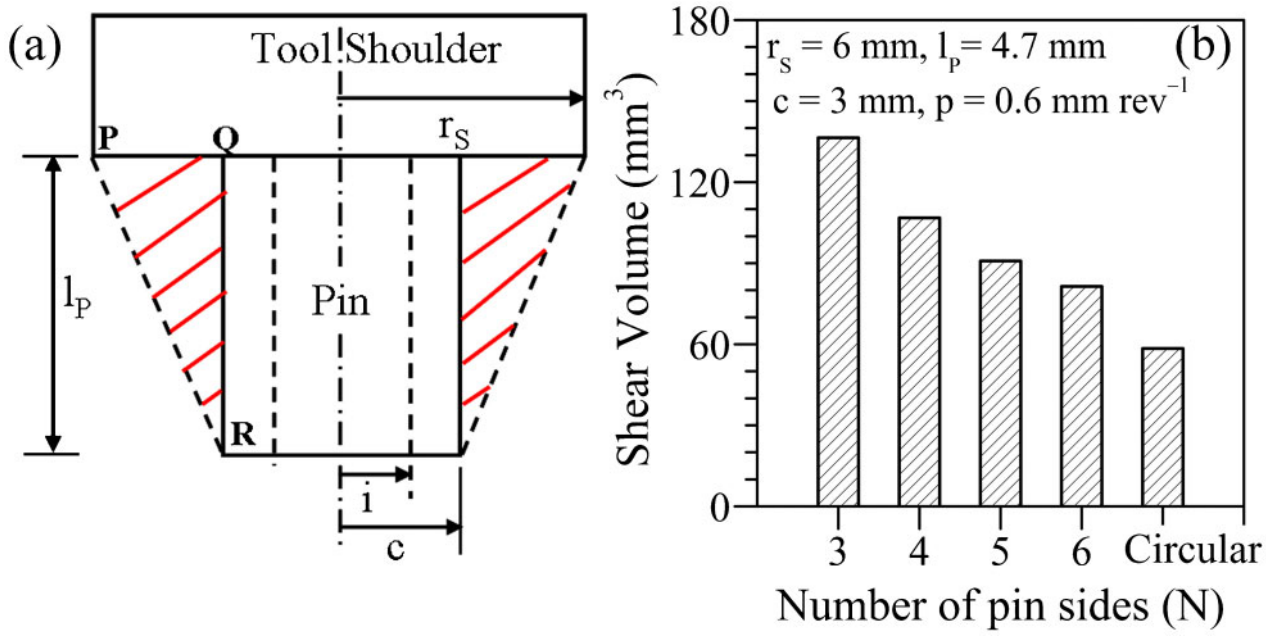

3 ***a*** **schematic presentation of plasticised (shear) region around FSW tool pin; and** ***b*** **variation of shear volume with number of polygonal pin sides for given** ***c*** **and** ***p*** **[21]**

independent experiments and the corresponding computed optimum pin profiles agree well for several cases in Table 1. For example, Ref. 21 in Table 1 reported FSW of an aluminium alloy AA2014 at a high weld pitch of 0·6 mm rev^{-1} and a circumradius of 3 mm. For these conditions, very marginal differences in the measured weld joint tensile strength were found with the square, pentagon and hexagon pin profiles. Equation (5) predicts a pentagonal pin to be the most optimum pin cross-section. Equation (5) also correctly predicts the circular cross-sections (N_P>6) for the welding of various alloys reported elsewhere.[17–20] In each of these cases, the weld pitch is very small and the reported as well as the corresponding estimated pin profiles are circular.

Table 1 also indicates welding conditions when the sticking of the plasticised material should not be a concern in the selection of the pin cross-section. When the heat generation rate per unit length of the weld is very high either due to high rotational speed of the tool or low welding velocity or both, significant softening of the work piece material is anticipated. In these cases, the flow of the workpiece material is facilitated by good plasticity of the material and the shear owing to the rotation of the tool pin becomes less critical in the orderly flow of the plasticised material. In Refs. 9–11 and 14–16, either the tool rotational speed is fairly high or the welding speed is quite low or both, and the sticking of the plasticised material to the tool does not

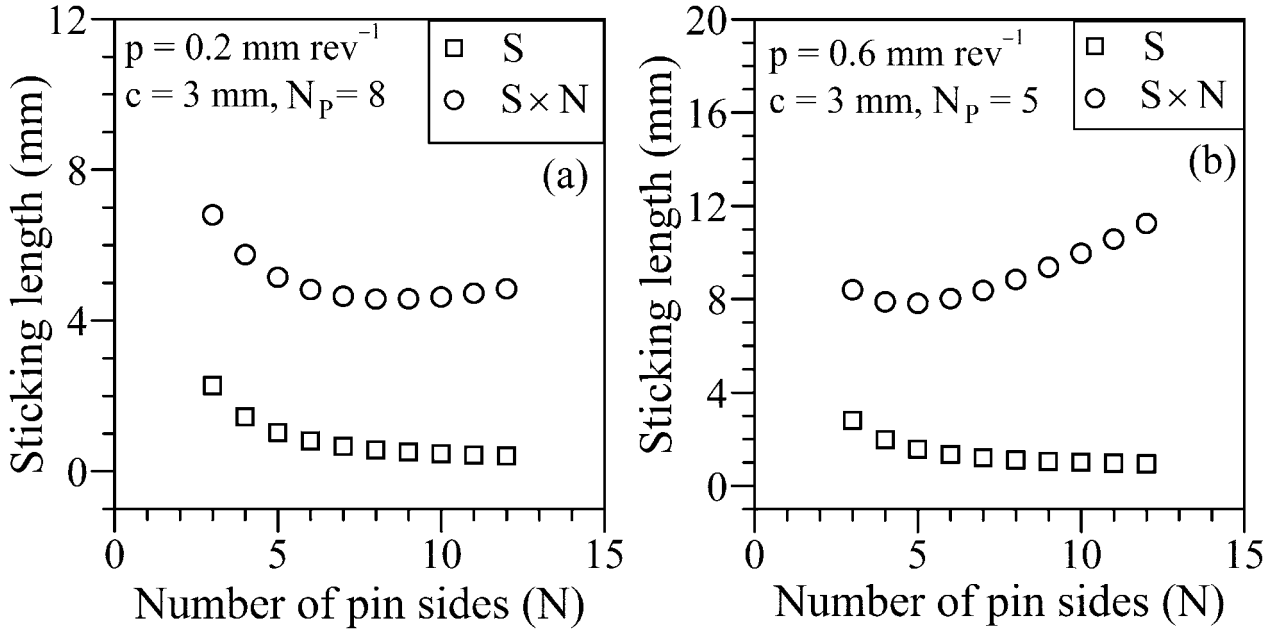

4 Variation of ***S*** **and (S × N) with number of pin sides for circumradius,** ***c*** **=3 mm and weld pitch,** ***p*** **, as** ***a*** **0·2 mm rev^{-1} and** ***b*** **0·6 mm rev^{-1} (Refs. 8 and 21)**

Table 1 Various non-circular pin profiles in FSW and estimated optimum pin sides*

Work material	Tool shape and size	Welding conditions			Experimental observation	N_{OPT}
		R/rev min^{-1}	v/mm s^{-1}	p/mm rev^{-1}		
Ref. 8; AA1050;	SD: 15 mm; SS: Smooth PD: 6 mm (c=3 mm) PL:				Highest weld joint UTS with	8, 8, 7, 5
t=5 mm	4·7 mm **PS**: SC, SCT (TP: 0·5 mm RHT), STr	1500	5·00, 6·25, 8·25, 11·67	0·20, 0·25, 0·33, 0·47	the **PS** as SC.	
Ref. 8; AA5083;		1500	0·5, 1·5, 3·25	0·02, 0·06, 0·13	with **PS** as STr.	27, 16, 11
t=5 mm		800	1·59, 3·33	0·12, 0·25	with **PS** as SCT.	11, 8
Ref. 9; AA1050;	SD: 14 mm; PL: 3·5 mm PD: 5 mm (c=2·5 mm)	1500	1·66	0·07	Highest nugget hardness	13
t=5 mm	**PS**: SC, SCT, STr, SSq				with the **PS** as SSq.	
Refs. 10 and 11;	SD: 18 mm; PL: 5·5 mm PD: 6 mm (c=3 mm)	1200	1·25	0·06	Highest weld joint UTS with	16
AA6061; t=6 mm	**PS**: SC, TC, SCT, STr, SSq				the **PS** as SSq.	
Ref. 12; MMC;	SD: 16 mm; PD: 5·71 mm (c=2·855 mm); **PS**:	2000	0·5	0·02	Highest weld joint UTS with	26
t=6 mm	SSq, TSq SHex, THex, SOct, TOct				the **PS** as SSq.	
Ref. 14; AA5083+	SD: 18 mm; SS: Flat PL: 5·7 mm; PD: 6·0 mm	950	1·0	0·06	Highest weld joint UTS with	16
AA6351; t=6 mm	(c=3 mm) **PS**: SSq, TSq, SHex, SOct, TOct	1300	1·0	0·05	the **PS** as SSq.	17
		600	1·0	0·10	with **PS** as SHex	12
Refs. 15 and 16;	SD: 18 mm; PL: 5·7 mm PD: 6 mm (c=3 mm)	1500, 1600, 1700	0·76	~0·03	Highest weld joint UTS with	22
AA2219; t=6 mm	**PS**: SC, TC, SCT, STr, SSq	1600	1·25	0·05	the **PS** as SSq	17
Ref. 17; AA1080;	PD: 4·5 mm (c=2·25 mm); **PS**: SCT				Highest weld joint UTS with	7
t=5 mm	PD: 7·07 mm (c=3·54 mm); **PS**: SSq	1000	3·33	0·20	the **PS** as SCT (TP=1·1 mm)	9
Ref. 18; AZ31B;	SD: 15, 18 and 21 mm; PL: 5·7 mm; PD: 6 mm	1600	0·67	0·03	Highest weld joint UTS with	22
t=6 mm	(c=3 mm); **PS**: SC, TC, SCT, STr, SSq				the **PS** as SCT (TP: 1 mm)	
Refs. 19 and 20;	**PS** (PD): SC (5, 6 and 7 mm); TC (6, 8 and 10 mm);	1400	2·67	0·11	Highest weld joint UTS with	10 (c=2·5 mm)
AA; t=6 mm	TSq (8·48, 11·31 and 14·14 mm)				the **PS** as SC (PD: 5 mm)	
Ref. 21; AA2014;	SD: 12 mm; PL: 4·7 mm PD: 6 mm (c=3 mm);	1000	10	0·60	Variation in weld joint YS &	5
t=5 mm	**PS**: TC, TTr, TSq, TPen, THex				UTS is minimal for **PS** as TSq, TPen, THex.	

*SD: shoulder diameter; SS: shoulder shape; PD: pin diameter; PL: pin length; TP: thread pitch; LHT (RHT): left (right) hand thread; TP: thread pitch; **PS: pin shape** [SC: straight circular; SCT: straight circular threaded; TC: tapered circular; STr: straight triangular; TTr: tapered triangular; SSq: straight square; TSq: tapered square; TPen: tapered pentagon; SHex: straight hexagon; THex: tapered hexagon; SOct: straight octagon; TOct: tapered octagon].

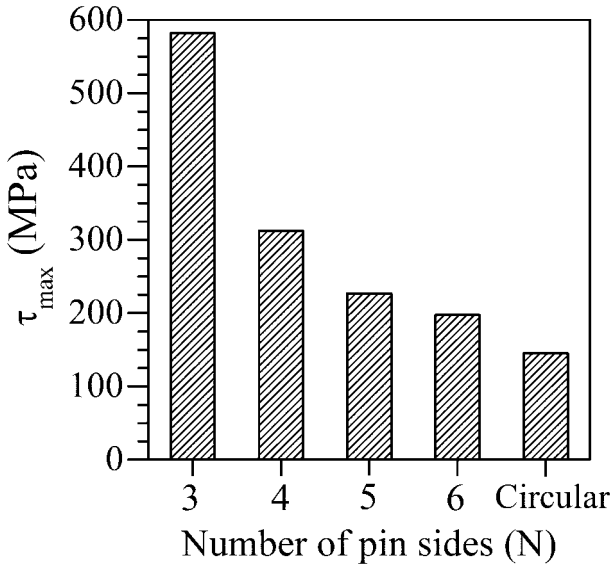

5 Variations in resultant maximum shear stress (τ_{max}) experienced by five different pin profiles with c=3 mm and p=0·46 mm rev^{-1} (tool rotational speed=1000 rev min^{-1} and welding speed=7·73 mm s^{-1}) during FSW of 5 mm thick AA2014

pose a major issue in the selection of the tool pin cross section. A similar observation can be made from the FSW of aluminium alloy AA1050 at different welding speeds reported elsewhere.[8] This study has investigated pins of both triangular and circular cross sections, and suggested circular cross-section as the desirable profile that has agreed reasonably well with the estimated pin profile from equation (5). For a harder material, AA5083, the authors have suggested the triangular and circular pins for p ranging from 0·02–0·13 mm rev^{-1} and 0·12–0·25 mm rev^{-1}, respectively while equation (5) estimated circular pins (N_P>6) for all values of p considered in this case. The theoretical calculations and the experimental results in Table 1 show that the optimum pin cross-sections for minimum adhesion in most cases are pins of large number of sides or circular cross-sections. While triangular or square cross-sections may be desirable for certain conditions, they are susceptible to significant adhesion of plasticised material.

Most of these investigations have recommended a suitable pin profile based on the measured tensile strength of the joint. What is interesting is that when the pin cross-sections are varied, the resulting variations of the weld joint hardness or tensile properties are often less than $\pm$15% in most cases.[9–11,21] While the experiments provided valuable data, the strength of the welded joint depends on the microstructure and the possible existence of flaws in the joint. The microstructure, in turn, is affected by the heating and cooling rates which depend on the welding variables. Although the pin geometry may play a role in the flow of the plasticised material and the integrity of the joint, many other important factors also affect weld properties. As a result, the measured values of mechanical properties cannot be attributed totally to the cross-section of the pin.

Impact of pin profile on tool durability

The effective stresses on the tool pins for a given FSW condition provide a measure of the durability of the respective tools for their continuous use without premature failure. Figure 5 shows the variation of τ_{max} for circular, triangular, square, pentagon and hexagon pin profiles for a typical FSW of AA2014 with a tool rotational speed of 1000 rev min^{-1} and welding speed of 7·73 mm s^{-1}, i.e. p=0·46 mm rev^{-1}. The computed values of τ_{max} following equation (6) are 582, 312, 226, 197 and 145 MPa for triangular, square, pentagon, hexagon and circular pin cross-sections. The decrease in τ_{max} with an increase in the number of sides for polygonal pins is attributed to the corresponding increase in their structural stiffness. For a given circumradius, c, the circular profile provides the highest value of structural stiffness and experiences the minimum value of τ_{max}. The ratio of the shear strength of the tool material and the corresponding τ_{max} is a measure of the durability of the tool pin. Considering a shear strength of 750 MPa for a typical FSW tool material EN40 steel,[34] the ability of the triangular, square, pentagon, hexagonal and circular pin cross-sections to safely endure the effective stress, on a relative basis is 1·3, 2·4, 3·3, 3·8 and 5·0, respectively. The triangular pin is the most susceptible to shear fracture compared to the other polygonal and the circular pins, particularly for the welding of hard alloys.

Conclusions

Various FSW tool pins of polygonal cross-sections were compared for their ability to avoid adhesion of plasticised material on the pin faces. It is shown that the pin geometry will have the highest impact at high ratio of welding speed to tool rotational speed (weld pitch). At low values of weld pitch, the pin profile does not have a significant impact. The optimum pin cross-section is circular at very low weld pitch, i.e. at high rotational speed and/or low welding speed. At high weld pitch, polygonal pins with fewer than six sides will be the optimum for minimum adhesion of plasticised material. The computed stresses on the tool pins of indicate that pins of circular cross-section will have lower stresses than the pins of polygonal cross-sections. Polygonal pins having larger number of sides will experience lower effective stresses.

Appendix

Considering a family of polygonal pin profiles confirming to a unique circumradius, c, the inradius, i, of any polygonal pin can be expressed in terms of the circumradius, c, as

$$i = c \times \cos\left(\frac{\pi}{N}\right) \tag{8}$$

Following theory of machining, the rake angle (β) of a polygonal pin in FSW can be estimated as function of number (N) of pin sides as $\beta = -\pi \times (N-2)/(2 \times N)$. Substituting equation (8) in equation (4), the latter can be rewritten as

$$S \times N = \frac{4}{3} N \left\{ c \left[1 - \cos\left(\frac{\pi}{N}\right) \right] + p \right\} \tag{9}$$

Expanding $\cos\left(\frac{\pi}{N}\right)$ and neglecting the higher order terms, equation (9) can be rewritten as

$$S \times N = \frac{4}{3} N \left[c \left(\frac{\pi^2}{2N^2} - \frac{\pi^4}{24N^4} \right) + p \right] \tag{10}$$

Next, considering the derivative of $(S \times N)$ with respect to N and equating it to zero leads to

$$N = \pm \frac{\pi}{2p^{1/2}} \times \left[c \pm \left(c^2 - 2pc\right)^{1/2}\right]^{1/2} \quad (11)$$

Equation (11) provides an unique solution for N with three realistic assumptions. First, N must be greater than zero. Second, a real solution of N exists only for c≥2p, which is intuitive as the circumradius for any polygonal pin is usually much greater than the linear distance moved by the tool pin in each revolution. Third, $\left[c - (c^2 - 2pc)^{1/2}\right]^{1/2}$ results in N to be lesser than 3 for the complete range of values of c and p used in contemporary FSW literature and hence, can be neglected. Thus, a realistic expression to estimate the number of pin sides (N_P) for a polygonal pin remains as

$$N_P = \frac{\pi}{2p^{1/2}} \times \left[c + \left(c^2 - 2pc\right)1/2\right]^{1/2} \quad (12)$$

A second order derivative of $(S \times N)$ with respect to N shows that

$$\frac{d^2(S \times N)}{dN^2} = \frac{4}{3}c\left(\frac{\pi^2}{N^3} - \frac{\pi^4}{2N^5}\right) \quad (13)$$

For $N = N_{OPT}$, the right hand side of equation (13) is always greater than zero when N≥3 for all practical values of c and p used in independent literature. Thus, equation (12) provides an optimum solution for a given value of c and p.

References

1. W. M. Thomas and E. D. Nicholas: 'Friction stir welding for the transportation industries', *Mater. Des.*, 1997, **18**, 269–273.
2. C. E. D. Rowe and W. M. Thomas: 'Advances in tooling materials for friction stir welding', Technical report, TWI, Cambridge, UK, 2005.
3. R. Rai, A. De, H. K. D. H. Bhadeshia and T. DebRoy: 'Review: friction stir welding tools', *Sci. Technol. Weld. Join.*, 2011, **16**, (4), 325–342.
4. P. A. Colegrove and H. R. Shercliff: 'CFD modelling of friction stir welding of thick plate 7449 aluminium alloy', *Sci. Technol. Weld. Join.*, 2006, **11**, (4), 429–441.
5. R. Zettler, S. Lomolino, J. F. dos Santos, T. Donath, F. Beckmann, T. Lippman and D. Lohwasser: 'Effect of tool geometry and process parameters on material flow in FSW of an AA2024-T351 alloy', *Weld. World*, 2005, **49**, (3/4), 41–46.
6. D. G. Hattingh, C. Blignault, T. I. van Niekerk and M. N. James: 'Characterization of the influences of FSW tool geometry on welding forces and weld tensile strength using an instrumented tool', *J. Mater. Process. Technol.*, 2008, **203**, (1–3), 46–57.
7. O. Lorrain, V. Favier, H. Zahrouni and D. Lawrjaniec: 'Understanding the material flow path of friction stir welding process using unthreaded tools'. *J. Mater. Process. Technol.*, 2010, **210**, (4), 603–609.
8. H. Fujii, L. Cui, M. Maeda and K. Nogi: 'Effect of tool shape on mechanical properties and microstructure of friction stir welded aluminum alloys', *Mater. Sci. Eng. A*, 2006, **A419**, (1–2), 25–31.
9. E. R. I. Mahmoud, M. Takahashi, T. Shibayanagi and K. Ikeuchi: 'Effect of friction stir processing tool probe on fabrication of SiC particle reinforced composite on aluminium surface', *Sci. Technol. Weld. Join.*, 2009, **14**, (5), 413–425.
10. K. Elangovan, V. Balasubramanian and M. Valliappan: 'Influences of tool pin profile and axial force on the formation of friction stir processing zone in AA6061 aluminium alloy', *Int. J. Adv. Manuf. Technol.*, 2008, **38**, 285–295.
11. K. Elangovan and V. Balasubramanian: 'Influences of tool pin profile and tool shoulder diameter on the formation of friction stir processing zone in AA6061 aluminium alloy', *Mater. Des.*, 2008, **29**, 362–373.
12. S. J. Vijay and N. Murugan: 'Influence of tool pin profile on the metallurgical and mechanical properties of friction stir welded Al-10 wt.10% TiB_2 metal matrix composite', *Mater. Des.*, 2010, **31**, (7), 3585–3589.
13. N. S. Sundaram and N. Murugan: 'Tensile behavior of dissimilar friction stir welded joints of aluminum alloys', *Mater. Des.*, 2010, **31**, (9), 4184–4193.
14. R. Palanivel, P. K. Mathews, N. Murugan and I. Dinaharan: 'Effect of tool rotational speed and pin profile on microstructure and tensile strength of dissimilar friction stir welded AA5083-H111 and AA6351-T6 aluminum alloys', *Mater. Des.*, 2012, **40**, 7–16.
15. K. Elangovan and V. Balasubramanian: 'Influences of pin profile and rotational speed of the tool on the formation of friction stir processing zone in AA2219 aluminum alloy', *Mater. Sci. Eng. A*, 2007, **A459**, 7–18.
16. K. Elangovan and V. Balasubramanian: 'Influences of tool pin profile and welding speed on the formation of friction stir processing zone in AA2219 aluminum alloy', *J. Mater. Process. Technol.*, 2008, **200**, 163–175.
17. M. Boz and A. Kurt: 'The influence of stirrer geometry on bonding and mechanical properties in friction stir welding process', *Mater. Des.*, 2004, **25**, 343–347.
18. G. Padmanaban and V. Balasubramanian: 'Selection of FSW tool pin profile, shoulder diameter and material for joining AZ31B magnesium alloy - An experimental approach', *Mater. Des.*, 2009, **30**, 2647–2656.
19. H. K. Mohanty, M. M. Mahapatra, P. Kumar, P. Biswas and N. R. Mandal: 'Effect of tool shoulder and pin probe profiles on friction stirred aluminum welds - a comparative study', *J. Marine Sci. Appl.*, 2012, **11**, 200–207.
20. H. K. Mohanty, M. M. Mahapatra, P. Kumar, P. Biswas and N. R. Mandal: 'Modeling the effects of tool shoulder and probe profile geometries on friction stirred aluminum welds using response surface methodology', *J. Marine Sci. Appl.*, 2012, **11**, 493–503.
21. K. Ramanjaneyulu, G. M. Reddy, A. V. Rao and R. Markandeya: 'Structure – property correlation of AA2014 friction stir welds: Role of tool pin profile', *J. Mater. Eng. Perform.*, 2013, **22**, (8), 2224–2240.
22. G. Buffa, D. Campanella and L. Fratini: 'On tool stirring action in friction stir welding of work hardenable aluminum alloys', *Sci. Technol. Weld. Join.*, 2013, **18**, (2), 161–168.
23. G. Buffa, J. Hua, R. Shivpuri and L. Fratini: 'Design of the friction stir welding tool using the continuum based FEM model', *Mater. Sci. Eng. A*, 2006, **A419**, (1–2), 381–388.
24. L. Fratini, G. Buffa, D. Palmeri, J. Hua and R. Shivpuri: 'Material flow in FSW of AA7075-T6 butt joints: numerical simulation and experimental verification', *Sci. Technol. Weld. Join.*, 2006, **11**, 412–421,
25. A. B. Chattopadhyay: 'Machining and machine tools', 84–115; 2000, New Delhi, Wiley India Pvt. Ltd.
26. N. A. Abukhshim, P. T. Mativenga and M. A. Sheikh: 'An investigation of the tool–chip contact length and wear in high–speed turning of EN19 steel', *J. Eng. Manuf.*, 2004, **218**, (8), 889–903.
27. A. Fatima and P. T. Mativenga: 'A review of tool–chip contact length models in machining and future direction for improvement', *J. Eng. Manuf.*, 2013, **227**, (3), 345–356.
28. M. Y. Friedman and E. Lenz: 'Investigation of the tool–chip contact length in metal cutting', *Int. J. Mach. Tool Des. Res.*, 1970, **10**, 401–416.
29. A. O. Tay, M. G. Stevenson, G. de. V. Davis and P. L. Oxley: 'A numerical method for calculating temperature distributions in machining from force and shear angle measurements', *Int. J. Mach. Tool Des. Res.*, 1976, **16**, 335–349.
30. A. Arora, M. Mehta, A. De and T. DebRoy: 'Load bearing capacity of tool pin during friction stir welding', *Int. J. Adv. Manuf. Technol.*, 2012, **61**, 911–920.
31. T. DebRoy, A. De, H. K. D. H. Bhadeshia, V. D. Manvatkar and A. Arora: 'Tool durability maps for friction stir welding of an Aluminum Alloy', *Proc. R. Soc. A*, 2012, **468A**, 3552–3570.
32. M. Mehta, A. De and T. DebRoy: 'Probing load bearing capacity of circular and non-circular tools in friction stir welding', Trends in Welding Research, Proc. 9th Int. Conf., 563–571; 2013, Materials Park, OH, ASM International.
33. 'Standard test method for short-beam strength of polymer matrix composite materials and their laminates', ASTM standard D2344/D2344M, ASTM International, West Conshohocken, PA, USA, 2013, 1–8.
34. J. Woolman and R. A. Mottran: 'The mechanical and physical properties of the British Standard EN steels (BS 970–1955)', Volume 3 (EN 40 to EN363), 1–29; 1969, Oxford, Pargaon Press.